A Wide Passband Ratio and Low-Complexity X-Band SIW Dual-Band Bandpass Filter

Van Dung Tran[1], Van Son Nguyen[2,*], Xuan Phuc Dao[2], Thi Hanh Quach[2], Thanh Trung Vu[1], The Hoang Nguyen[1], Van Ba Nguyen[1] and Hai Anh Ngo[3]

[1]*Institute for Technology Development Media and Community Assistance (IMC), 100000 Hanoi, Vietnam*
[2]*Faculty of Electrical and Electronic Engineering, Hanoi Open University (HOU), 100000 Hanoi, Vietnam*
[3]*Institute of Information Technology, VietNam Academy of Science and Technology (VAST), 100000 Hanoi, Vietnam*

_____

Abstract

This paper presents a dual-band bandpass filter (BPF) operating at 9.5 GHz and 11 GHz using a substrate integrated waveguide (SIW) technology. The filter was designed on the diplexer structure to enable the flexible control of the spacing of two passbands. By carefully designing the input/output cavities, spacing between two passbands can be adjusted freely. In addition, thanks to the design of each branch cavity, performance of each band is able to tune easily. The filter was designed on a cost-effective RO4003C substrate and simulated using a CST Microwave Studio 2019 simulator based on the time-domain analysis. The simulated insertion losses at 9.5 GHz and 11 GHz are 2.0 and 1.9 dB, respectively whereas the return losses at these two center frequencies are -15.7 dB and 32.8 dB, respectively. The fractional bandwidth of 1-dB insertion loss is 3.7 % and 3.6 % at the two passbands. The total size of the filter is just 2.4 x 3.5 mm^2. The proposed filter aims at using for next-generation wireless communications such as satellite communication, 5G, 6G and beyond.

Keywords: Bandpass filter (BPF), Substrate integrated waveguide (SIW), RO4003C substrate, CST Studio, CSRR, X-band, Diplexer, VIA diameter.

_____

1. Introduction

Dual-band BPF is now becoming critical in various modern wireless communication systems to meet the requirements of the multi-band and multimode operation. Lots of methods have been introduced to design the dual-band BPF operating at different frequency bands. The BPF can be designed in waveguide, microstrip and substrate integrated waveguide (SIW) technologies. Waveguide filter offers the advantages of the low-loss, and high-power capability but at the cost of bulky and hard to integrate [1-6]. The microstrip technology, on the other hand, provides a light weight and easy integration capabilities with the planar platforms [7-12]. However, the downside of the microstrip filters is the high-loss at high frequencies and low power handling capabilities. SIW technology is recently emerging as a promising candidate to replace waveguide filters and microstrip filters because it can deliver a relatively low-loss at high frequencies with a light weight and high-power capability. Many studies on the SIW filters have been widely reported [13-20]. A variety of studies on the dual-band SIW BPFs at different frequency bands has been reported [21-24]. In [21], authors propose a novel dual-band BPF operating at X-band using complementary split-ring resonators (CSRR) structure. By using the CSRR structure, this type of filter offers a compact size with a low insertion loss of 1.5 dB and 1.9 dB at each band. However, the downside of this dual-band filter is the narrow bandpass ratio of 1.12. Another dual-band CSRR SIW BPF is reported in [22]. By using a several perturbed vias, the passband ratio can be increased to 1.37 at the higher X-band of 9.8 GHz and 13.5 GHz. The input return loss, however, is degraded due to the poor matching of the slot lines. A high passband ratio of 2.49 SIW BPF was reported in [23]. Although this filter was also realized on the CSRR structure with a low insertion loss, it only operates at the low frequencies of 1.94 GHz and 4.84 GHz. In [24], authors propose a dual-band BPF using the perturbed SIW circular cavity with a high bandpass ratio of 1.25 and low insertion loss. Nevertheless, this filter operates at the lower X-band because of the high radiation loss near the frequency bands due to the use of the slot lines. In this paper, to realize a dual-band BPF with a high passband ratio, low insertion loss and compactness, a dual-band SIW BPF using rectangular cavities based on the diplexer concept is presented. By using such a method, the passband ratio can be controlled flexibly by setting resonant frequencies of the input and output resonators. In addition, performance of each band filter can be also optimized by adjusting parameters of the channel cavities. The rest of the paper is organized as follows: The next section presents strategy to design the dual-band BPF, after that the simulations of the filter are conducted in the third section, the final section concludes the paper.

2. Design Strategy of the Dual-Band BPF

The proposed BPF is designed on the diplexer concept where its block diagram is described in Fig. 1. The filter is composed of 4 SIW cavities, namely (1) – (4), with two identical input and output cavities, (1) and (4). The input/output cavity resonates at f_1 (9.5 GHz) and f_2 (11 GHz) for TE_{101} and TE_{201} modes, respectively. After that, each cavity is employed on each channel of the diplexer filter. The upper (2) and lower (3) cavities are designed to resonate at f_1 and f_2 for the TE_{101} mode, respectively.
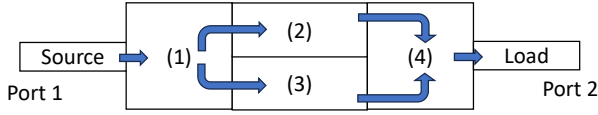
Fig. 1. Block diagram of the dual-band BPF

By using such a diplexer filter design method, the dual-band BPF centered at f_1 and f_2 can be easily realized. The passband ratio can be tuned by controlling the resonant frequencies f_1 and f_2 of the input and output cavities. This is in turn can be determined by tuning dimensions of these cavities. Performance of the filter at each band can be determined by the Q-factor and bandwidth of each channel cavity.

3. Implement and Simulation of the Dual-Band BPF

To implement the filter, each cavity needs to be constructed first where the input/output (IO) cavity plays a critical role as it contributes to the passband ratio as well as the insertion loss in each band. In this study, IO cavity is a rectangular SIW cavity, its structure along with the channel cavities, (2) and (3) are given in Fig. 2. It is necessary to employ two 50 Ω lines at two ends of the filter to connect the filter with the source and the load. The filter is constructed in the CST Microwave Studio simulator.
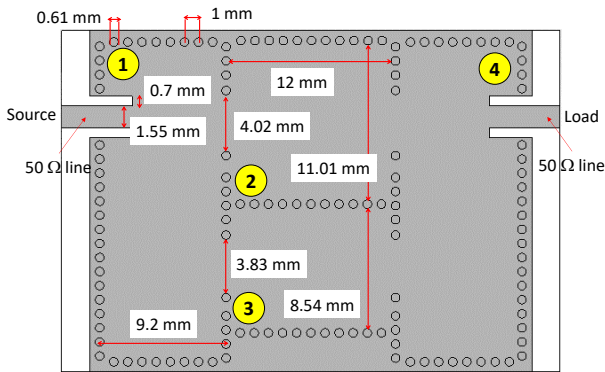

Fig. 2. Structure of the proposed filter in CST Microwave Studio simulator

It is important to note that the diameter of the VIA holes and the spacing between adjacent vias are designed to meet the requirement of low radiation loss in the SIW waveguide. The input and output cavities have identical dimensions. Their dimensions determine the resonant frequency of the cavity. The resonant frequency of an SIW cavity is given as [25]:

$$f_{r(TEm0n)} = \frac{c}{2\sqrt{\varepsilon_r}} \sqrt{\left(\frac{m}{W_{eff}}\right)^2 + \left(\frac{n}{L_{eff}}\right)^2} \qquad (1)$$

where $f_{r(TEm0n)}$ is the resonant frequency of TE_{m0n} mode, c is speed of light in vacuum, ε_r is the relative dielectric constant of the dielectric substrate, W_{eff} and L_{eff} are effective width and length of the SIW structure and they are given as follows:

$$W_{eff} = W - \frac{d^2}{0.95s} \qquad (2)$$

$$L_{eff} = L - \frac{d^2}{0.95s} \qquad (3)$$

where W and L are the equivalent width and length of a hollow rectangular waveguide and d is diameter of the VIA holes in SIW structure. In Eq.1, m and n are integer numbers indicating the operation mode. Hence, it can be noticed that, width, length and VIA diameter determine the resonant frequency of the SIW cavity. Fig. 3 shows the dependence of the resonant frequencies of TE_{101} mode and TE_{201} mode on the width of the IO cavity with the length of 26 mm and the VIA diameter of 0.61 mm.
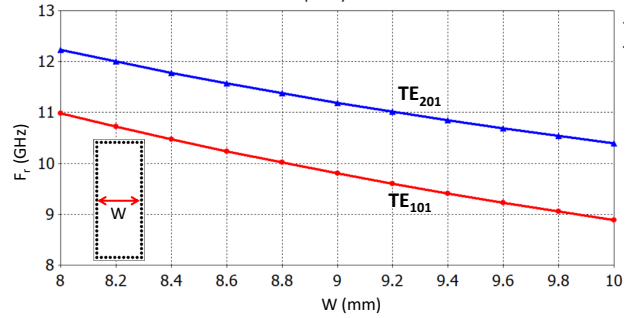

Fig. 3. Dependence of the resonant frequency of the IO cavity on its width for a fixed length and VIA hole's diameter

From this figure, width of the IO cavity can be determined to be 9.2 mm for the resonant frequencies of 9.5 GHz and 11 GHz. These resonant frequencies are the center frequencies of the dual-band BPF. Fig. 4 illustrates the electric field distribution in the IO cavity for the TE_{101} mode at 9.5 GHz and TE_{201} mode at 11 GHz. It can be observed the appropriate field distribution in the cavity.
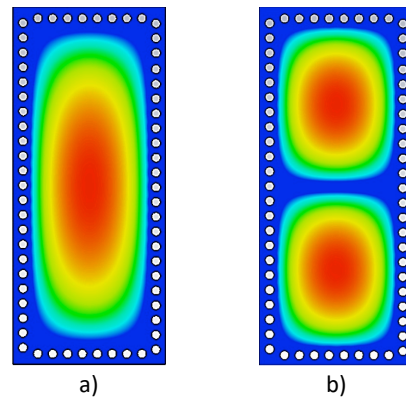

Fig. 4. Electric field distribution in the IO cavity: a) resonant mode of TE_{101} at 9.5 GHz, b) resonant mode of TE_{201} at 11 GHz

After the IO cavity has been designed correctly, the channel cavity (2) and (3) are then constructed. It is noticed that dimensions of these cavities are calculated so that they resonate at each resonant frequency of the IO cavity. In other words, the cavity (2) will resonate at 9.5 GHz and the cavity (3) resonates at 11 GHz.

Fig. 5 and Fig. 6 describe the dependence of the resonant frequency and Q-factor of TE_{101} mode on the width of the channel cavity for a fixed length of 12 mm and VIA hole's diameter of 0.61 mm.
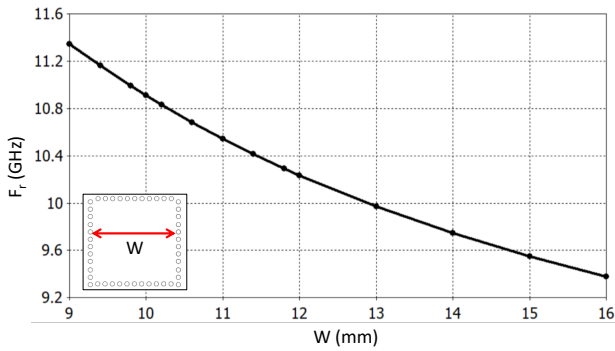
Fig. 5. Dependence of the resonant frequency of the channel cavity on its width for a fixed length and VIA hole's diameter
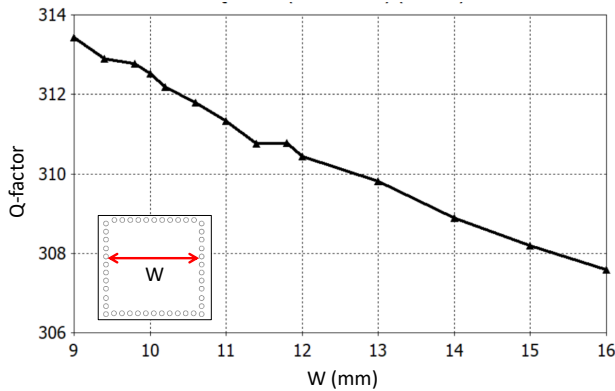

Fig. 6. Dependence of the Q-factor of the channel cavity on its width for a fixed length and VIA hole's diameter

From these figures, the widths of each channel cavity can be determined to be 15.3 mm for the resonant frequency and Q-factor of 9.5 GHz and 308 and 9.8 mm for the resonant frequency and Q-factor of 11 GHz and 312. Fig. 7 shows the electric field distribution in these cavities regarding the resonant modes of TE_{101}.
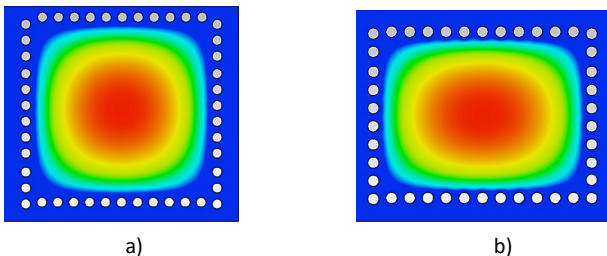

Fig. 7. Electric field distribution in the channel cavities: a) resonant mode of TE_{101} at 11 GHz in cavity (3), b) resonant mode of TE_{101} at 9.5 GHz in cavity (2)

After all the individual cavities including IO cavity and channel cavities have been successfully designed, the final filter as shown in Fig. 2 is then tested by an EM simulation in the CST Microwave Studio 2019 simulator using a time domain analysis using an adaptive meshing function to ensure a high accuracy of simulations. Fig. 7 shows the simulated frequency response of the proposed filter. It can be clearly seen a dual passband of 9.5 GHz and 11 GHz.

The insertion losses at 9.5 GHz and 11 GHz are 2.0 and 1.9 dB, respectively whereas the return losses at these two center frequencies are -15.7 dB and -32.8 dB, respectively. At the center frequency of 9.5 GHz, the fractional bandwidth of 1-dB insertion loss is 3.7 % whereas this value at 11 GHz is 3.6 %.

To validate the accuracy of data shown in Fig. 8, it is essential to display the field distribution in the filter at the two center frequencies to ensure the correct operation of the filter.
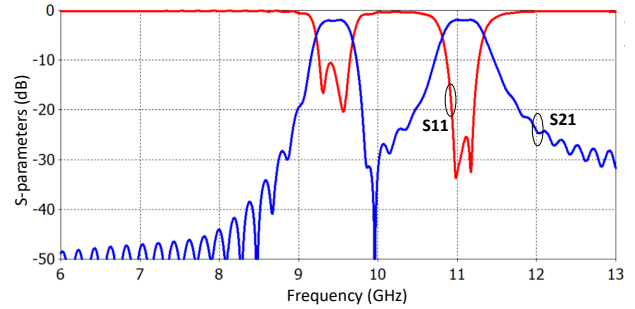

Fig. 8. Simulated frequency response of the proposed dual-band filter
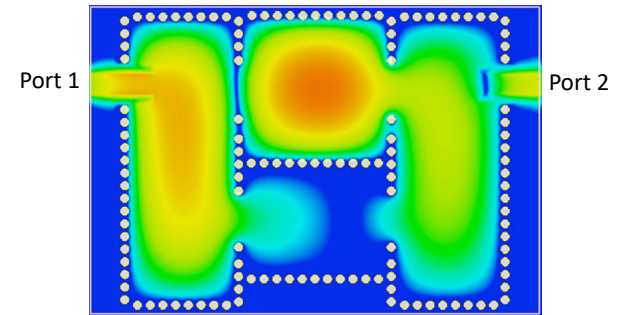

Fig. 9. Electric field distribution in the filter at 9.5 GHz

Fig. 9 shows the electric field distribution in the filter at 9.5 GHz. As expected, the IO cavity resonates at TE_{101} mode at 9.5 GHz and the signal goes through the 9.5-GHz channel that is the cavity (2) path. Similarly, Fig. 10 indicates the electric field in the filter at 11 GHz. In this case, the IO cavities resonate at 11 GHz for the TE_{201} mode whereas the cavity (3) resonates at 11 GHz for the TE_{101} mode. These considerations confirm the accuracy of the filter design.
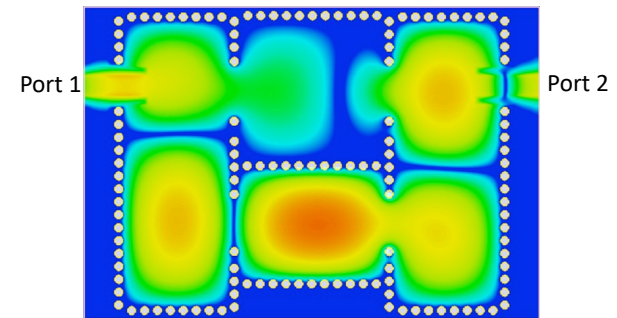

Fig. 10. Electric field distribution in the filter at 11 GHz

Tab. 1 lists the comparison of the proposed filter with other state of the art dual-band BPF.

Table 1. Comparison of the proposed BPF with other reported state of the art dual-band BPFs

Works	CF (GHz)	IL (dB)	RL (dB)	Resonator Type
[4]	7.89/8.89	1.5/1.9	-15/-15	SIW + CSRR
[5]	9.8/13.5	1.8/1.5	-9.8/-10.6	SIW + CSRR
[6]	7.7/9.6	1.9/1.6	-10/-11	SIW
[7]	1.9/4.8	1.2/2.7	-15/-16	SIW
This work	*9.5/11*	*2.0/1.9*	*-15/-32*	*SIW*

From the table, it can be seen that the proposed filter offers a low-complexity, a relatively wide passband ratio at the higher X-band with good return losses at two passbands.

4. Conclusion

This paper presents a design of a low-complexity dual-band SIW BPF using the diplexer-like method. The IO cavities are designed to realize a wide passband ratio whereas each channel cavity is adjusted to obtain the desired performance in each passband. The simulated results indicate the proposed filter operates at two center frequencies of 9.5 GHz and 11 GHz with a FBW of 3.7 % and 3.6 %, respectively. The return losses at these two center frequencies are -15.7 dB and -32.8 dB. Compared with other state of the art dual-band BPFs, the proposed filter offers a relatively wide passband ratio at the higher X-band with good return losses at two passbands and a low-complexity. With these promising results, the designed filter can be used for the next-generation wireless communications such as satellite communication, 5G, 6G and beyond.

References

[1]. H. Nimehvari Varcheh and P. Rezaei, "Low-loss X-band waveguide bandpass filter based on rectangular resonators," *Microw. Opt. Techn. Let.*, vol. 64, no. 4, pp. 701-706, Apr. 2022.

[2]. H. Liu, F. Zhang, C. Guo, B. Xue, and J. Xu, "An X-band waveguide bandpass filter with enhanced stopband using offset resonators," *IEICE Electr. Expr.*, vol. 18, no. 2, pp. 20200406-20200406, Jan. 2021.

[3]. C. Guo, X. Shang, M. J. Lancaster, and J. Xu, "A 3-D printed lightweight X-band waveguide filter based on spherical resonators," *IEEE Microw. Wirel. Comp. Let.*, vol. 25, no. 7, pp. 442-444, Jun. 2015.

[4]. R. Dahle, P. Laforge, and J. Kuhling, "3-D printed customizable inserts for waveguide filter design at X-band," *IEEE Microw. Wirel. Comp. Let.*, vol. 27, no. 12, pp. 1080-1082, Oct. 2017.

[5]. V. E. Boria and B. Gimeno, "Waveguide filters for satellites," *IEEE Microç. Magaz.*, vol. 8, no. 5, pp. 60-70, Oct. 2007.

[6]. G. Macchiarella, G. G. Gentili, C. Tomassoni, S. Bastioli, and R. V. Snyder, "Design of waveguide filters with cascaded singlets through a synthesis-based approach," *IEEE Trans. Microw. Th. Techn.*, vol. 68, no. 6, pp. 2308-2319, Feb. 2020.

[7]. J.-T. Kuo, T.-H. Yeh, and C.-C. Yeh, "Design of microstrip bandpass filters with a dual-passband response," *IEEE Trans. Microw. Th. Techn.*, vol. 53, no. 4, pp. 1331-1337, Apr. 2005.

[8]. H. Xu and W. Sheng, "The X-band microstrip filter design," in *2017 7th IEEE International Symposium on Microwave, Antenna, Propagation, and EMC Technologies (MAPE)*, Oct. 2017, pp. 351-355.

[9]. B. Adli, R. Mardiati, and Y. Y. Maulana, "Design of microstrip hairpin bandpass filter for X-band radar navigation," in *2018 4th International Conference on Wireless and Telematics (ICWT)*, Jul. 2018, pp. 1-6.

[10]. M. H. Masood and S. B. Suseela, "Compact bandpass filter with reconfigurable X-band using stepped impedance resonator and folded structure," *J. Eng.*, vol. 2018, no. 3, pp. 162-165, Mar. 2018.

[11]. C. Y. Ng, M. Chongcheawchamnan, M. Aftanasar, I. Robertson, and J. Minalgiene, "X-band microstrip bandpass filter using photoimageable thick-film materials," in *2002 IEEE MTT-S International Microwave Symposium Digest* (Cat. No. 02CH37278), Jun. 2002, vol. 3, pp. 2209-2212.

[12]. B. Dong, Q. Feng, and S. Yang, "Research and design of X-band SIR microstrip filters," in *2009 International Conference on E-Business and Information System Security*, May 2009, pp. 1-4.

[13]. X.-P. Chen and K. Wu, "Substrate integrated waveguide filters: Design techniques and structure innovations," *IEEE Microç. Magaz.*, vol. 15, no. 6, pp. 121-133, Sep. 2014.

[14]. A. Iqbal, J. J. Tiang, S. K. Wong, M. Alibakhshikenari, F. Falcone, and E. Limiti, "Miniaturization trends in substrate integrated waveguide (SIW) filters: A review," *IEEE Acc.*, vol. 8, pp. 223287-223305, Dec. 2020.

[15]. Z. Hao, W. Hong, H. Li, H. Zhang, and K. Wu, "A broadband substrate integrated waveguide (SIW) filter," in *2005 IEEE antennas and propagation society international symposium*, Jul. 2005, vol. 1, pp. 598-601.

[16]. Y. D. Dong, T. Yang, and T. Itoh, "Substrate integrated waveguide loaded by complementary split-ring resonators and its applications to miniaturized waveguide filters," *IEEE Trans. Microw. Th. Techn.*, vol. 57, no. 9, pp. 2211-2223, Aug. 2009.

[17]. F. Mira, J. Mateu, and C. Collado, "Mechanical tuning of substrate integrated waveguide filters," *IEEE Trans. Microw. Th. Techn.*, vol. 63, no. 12, pp. 3939-3946, Oct. 2015.

[18]. F. Zhu, W. Hong, J.-X. Chen, and K. Wu, "Cross-coupled substrate integrated waveguide filters with improved stopband performance," *IEEE Microw. Wirel. Comp. Let.*, vol. 22, no. 12, pp. 633-635, Nov. 2012.

[19]. C. Tomassoni, L. Silvestri, A. Ghiotto, M. Bozzi, and L. Perregrini, "Substrate-integrated waveguide filters based on dual-mode air-filled resonant cavities," *IEEE Trans. Microw. Th. Techn.*, vol. 66, no. 2, pp. 726-736, Jan. 2018.

[20]. L. Silvestri, E. Massoni, C. Tomassoni, A. Coves, M. Bozzi, and L. Perregrini, "Substrate integrated waveguide filters based on a dielectric layer with periodic perforations," *IEEE Trans. Microw. Th. Techn.*, vol. 65, no. 8, pp. 2687-2697, Jun. 2017.

[21]. H. Zhang, W. Kang, and W. Wu, "Dual-band substrate integrated waveguide bandpass filter utilising complementary split-ring resonators," *Electr. Lett.*, vol. 54, no. 2, pp. 85-87, Jan. 2018.

[22]. L. F. Shi, C. Y. Sun, C. Chen, G. X. Liu, and Y. F. Shi, "Dual-band substrate integrated waveguide bandpass filter based on CSRR s and multimode resonator," *Int. J. RF Microw. Comp.-Aid. Eng.*, vol. 28, no. 9, p. e21412, Nov. 2018.

[23]. A. R. Azad and A. Mohan, "Single-and dual-band bandpass filters using a single perturbed SIW circular cavity," *IEEE Microw. Wirel. Comp. Let.*, vol. 29, no. 3, pp. 201-203, Feb. 2019.

[24]. B. Yin and Z. Lin, "A novel dual-band bandpass SIW filter loaded with modified dual-CSRRs and Z-shaped slot," *AEU-Int. J. Electr. Communic.*, vol. 121, p. 153261, Jul. 2020.

[25]. Y. Cassivi, L. Perregrini, P. Arcioni, M. Bressan, K. Wu, and G. Conciauro, "Dispersion characteristics of substrate integrated rectangular waveguide," *IEEE Microw. Wirel. Comp. Let.*, vol. 12, no. 9, pp. 333-335, Sep. 2002.